Boundary-Layer Meteorol (2008) 127:97–110
DOI 10.1007/s10546-007-9256-8

ORIGINAL PAPER

# Influence of a Two-scale Surface Roughness on a Neutral Turbulent Boundary Layer

**Pietro Salizzoni · Lionel Soulhac · Patrick Mejean · Richard J. Perkins**

Received: 4 June 2007 / Accepted: 13 December 2007 / Published online: 19 January 2008
© Springer Science+Business Media B.V. 2008

**Abstract** Flow in the urban boundary layer is strongly influenced by the surface roughness, which is composed principally of isolated buildings or groups of buildings. Previous research has shown that the flow regime depends on the characteristic height of these obstacles ($H$), and the spacing between them ($W$). In reality, the urban boundary layer contains roughness elements with a wide range of length scales; in many practical situations these can be classified into large-scale roughness—buildings, or groups of buildings—and small-scale roughness, such as street furniture and elements on the façades and roofs. It is important to understand how the small-scale roughness might modify mass and momentum transfer in the urban boundary layer, but relatively little information is available concerning the potential interaction between large- and small-scale roughness elements in the different flow regimes. This problem has been studied using wind-tunnel experiments, by measuring vertical velocity profiles over a two-dimensional obstacle array, adding small-scale roughness elements to the top of larger parallel square bars. The experiments were performed for different cavity aspect ratios: the results show that the small-scale roughness increases the turbulence intensities and the momentum transfer when the large-scale obstacles are closely packed ($H/W > 1$) but it has very little effect for more widely-spaced obstacles ($H/W < 1$).

**Keywords** Roughness · Turbulent boundary layer · Urban canopy flow

P. Salizzoni (✉) · L. Soulhac · P. Mejean · R. J. Perkins
Laboratoire de Mécanique des Fluides et d'Acoustique, Université de Lyon UMR CNRS 5509 – Ecole Centrale de Lyon, INSA Lyon, Université Claude Bernard Lyon I, 36, Avenue Guy de Collongue, 69134 Ecully, France
e-mail: pietro.salizzoni@polito.it

P. Salizzoni
Dipartimento di Ingegneria Aeronautica e Spaziale, Politecnico di Torino, Corso Einaudi, 24, 10129 Torino, Italy

## 1 Introduction

The mean and turbulent wind velocities in the urban boundary layer are strongly influenced by the surface roughness that depends on the dimensions and positions of the buildings. Increasingly this information is available, at high resolution, from GIS databases, but it is often too detailed to be used directly in operational models. It is therefore necessary to find ways of characterizing the influence of these obstacles on the flow—the aerodynamic roughness—exploiting all the available information as much as possible. This is not a new problem; Nikuradse (1933) performed a set of systematic experiments using isolated sand grains to determine the relationship between the size of individual roughness elements and their influence on the flow. But the urban surface is different from many 'natural' surfaces, in that it is generally composed of obstacles with distinctly separate scales—the buildings themselves, and then the various features (chimneys, aerials, balconies etc.) that modify the basic form of the buildings. There has only been limited studies of this problem; Rafailidis (1997), for example, investigated the influence of slanted roofs on the dynamics of the lower part of a neutral turbulent boundary layer.

It is generally assumed that the velocity profile in a neutral turbulent boundary layer can be divided into two regions—an inner region, in which the flow depends on surface properties, and an outer layer in which the relevant scales are the depth of the boundary layer and the free stream velocity. If the scales are chosen correctly the scaled profiles in each region can be described by some form of similarity solution. These two similarity solutions must match at the interface between the two regions (Tennekes and Lumley 1972), and an important consequence of this requirement is the result that there is an intermediate zone, between the inner and the outer layers, where the velocity profile must have a logarithmic form:

$$\frac{U}{u_*} = \frac{1}{\kappa} \ln \frac{z-d}{z_o}, \tag{1}$$

where $u_*(= \sqrt{-\tau_0/\rho})$ is the friction velocity, $\kappa$ is the von Kármán constant and $z_0$ is the roughness length. The parameter $d$ is the displacement height, to take account of the fact that the vertical origin of the velocity profile does not necessarily coincide with the physical origin chosen for the coordinate system.

It is worth noting that in Eq. 1 the mean velocity $U$ depends only on the vertical coordinate $z$; this implies the assumption of homogeneity of the flow field on the horizontal planes. Of course, because of the variation created by individual roughness elements, this cannot be true close to the surface, except in a statistical sense. We can therefore define a height—the blending height, $z_*$—above which the flow is homogeneous in the horizontal plane. The region below $z_*$, in which the flow is influenced by the drag exerted by individual obstacles, and by the form of their wakes, is referred to as the roughness sub-layer (RSL).

Early studies of rough wall turbulent boundary layers showed that the roughness length scale depends on both the height of the roughness elements and the spacing between them (Raupach 1992; Raupach et al. 2006) and the flow regimes can be classified on the basis of the aspect ratio $H/W$ of the obstacles (Perry et al. 1968; Oke 1987). This classification is based essentially on the length scales $H$ and $W$ that characterize the largest roughness elements. The urban surface is often composed of large roughness elements modified by much smaller elements, with distinct length scales. So the the first question is whether, in such circumstances, a single length scale is sufficient to characterize the surface roughness. A second question to be addressed is how to define such a roughness scale, as a function of the different surface length scales. Specifically, we need to examine how the presence of smaller elements modifies the flow regimes and the similarity profiles that have been measured for

single scale roughness. It is likely that the influence of the small-scale roughness will vary, depending on the type of flow regime created by the large-scale roughness. Similar studies have been conducted for hilly surfaces (Gong et al. 1996; Athanassiadou and Castro 2001) focusing on the influence of the small roughness on the location of flow separation downstream of a sinusoidal obstacle. The aim of this study is to investigate how the presence of small-scale roughness elements modifies the flow in a turbulent boundary layer over an urban-like roughness, and how this depends on the aspect ratio of the large-scale roughness elements.

## 2 Experimental Set-Up

The experiments were performed in a recirculating wind tunnel at the Laboratoire de Mécanique des Fluides et d'Acoustique at the Ecole Centrale de Lyon in France. The test section of the wind tunnel is 9 m long, 1 m high and 0.7 m wide, with glass side walls. To generate a boundary layer with characteristics similar to those of an atmospheric boundary layer, we used a combination of spires at the entrance to the test section and roughness blocks at the floor of the tunnel, as originally proposed by Counihan (1969) and Irwin (1981). In these experiments three spires with a height of 0.5 m were used. We have simulated an idealized street geometry consisting of a sequence of 2D parallel canyons, formed by a set of square section bars (0.06 m × 0.06 m) placed normal to the flow, as shown in Fig. 1. The length $L$ of the bars in the transverse direction was equal to 0.7 m, i.e. $L \approx 12H$. The influence of small-scale roughness was studied by adding 2D roughness elements (5 mm × 5 mm) to the tops of the bars.

The spacing between the bars could be varied, and experiments were performed for three values of the height-to-width ratio ($H/W = 1, 2, 1/2$); these will be referred to as Configuration 1, 2 and 3 respectively. According to the classification mentioned in the introduction, the first two configurations correspond to skimming flow (Oke 1987) or d-type roughness (Perry et al. 1968), whilst the third configuration corresponds to wake-interference flow (Oke 1987) or k-type roughness (Perry et al. 1968). In all three configurations the experiments were carried out first without the small-scale roughness (Configurations 1a, 2a and 3a) and then with the roughness (Configuration 1b, 2b, and 3b). Finally, in order to evaluate the effect of the 'small roughness' alone, we have studied another configuration (Configuration 0b) consisting of a plane wall covered in the small roughness elements. Figure 2 provides an overview of the different configurations. These configurations have been chosen for two main reasons—they

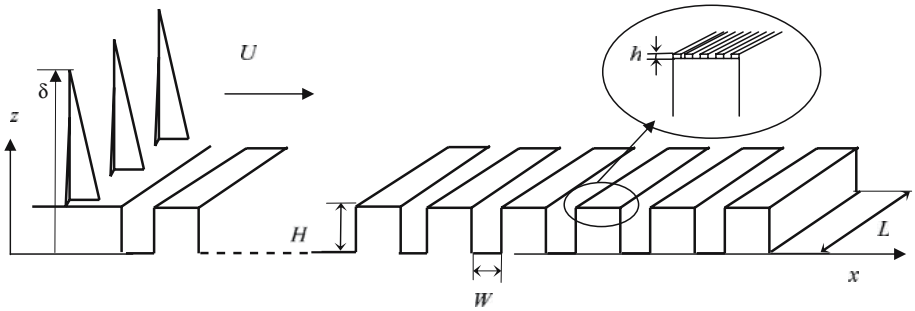


**Fig. 1** Overview of the wind-tunnel installation

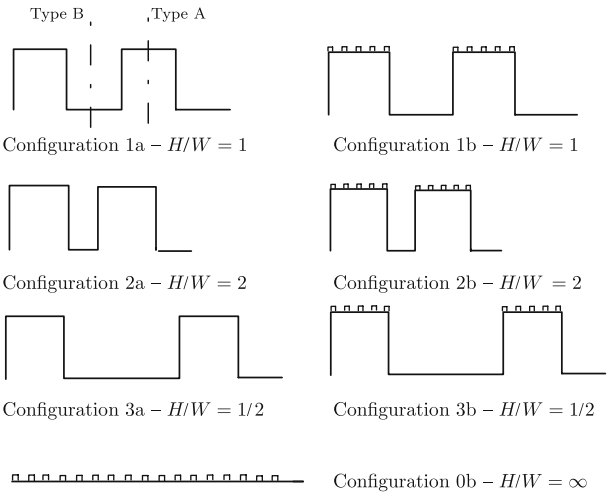


**Fig. 2** Geometrical configurations and vertical profile locations (Type A and Type B profiles)

are representative of typical street aspect ratios in urban areas (Soulhac 2000) and they enable us to compare flow dynamics in the skimming regime and wake-interference regime.

The wall geometry is characterized by the following length scales: the 2D obstacle height $H = 60\,\text{mm}$, the distance between the large obstacles $W$ ($30\,\text{mm} < W < 120\,\text{mm}$), the small-scale roughness at the top of the obstacles $h = 5\,\text{mm}$ and the distance between the small-scale roughness elements $l = 8.75\,\text{mm}$. The velocity profiles were measured at a distance equal to about 12 times the height of the vortex generators downstream of the entry to the test section. This means that the measurement positions were located within an interval for which we can assume that the development of coherent structures in the wake of the vortex generators has already reached an equilibrium condition and that the longitudinal scale related to the growth of the boundary layer is much larger than the boundary-layer depth. In these conditions, the dynamics of the flow will depend on the scales imposed at the wall and on another length scale only, related to the boundary-layer thickness $\delta$. The dimensions of the characteristic length scale of the simulated domain have been chosen to preserve a realistic ratio between the thickness of an adiabatic atmospheric boundary layer (which is of the order of 100 m), a typical building height (which is of the order of 10 m) and a smaller scale element at the top of the buildings such as a chimney or a roof (which is of the order of 1 m). The typical scale ratio between the wind-tunnel model and reality is 1/166.

## 3 Hot Wire Anemometry Velocity Measurements

Velocities were measured by hot wire anemometry, using a single probe and an X-probe functioning as a constant temperature anemometer. The diameter of the wire was $5\,\mu\text{m}$, and the acceptance angle of the X-probe was $\pm 45°$. For the three configurations, vertical profiles were measured at two locations (Fig. 2): above the obstacle mid-point—type A profile—and at the centre of the cavity—type B profile. In all cases the experiments were performed first without the small-scale roughness and then repeated with the additional small-scale roughness.

### 3.1 Boundary-Layer Parameters

To begin with, we have analyzed the measured velocity profiles to determine the characteristic boundary-layer parameters. In all cases the free stream velocity $U_\infty$ at the top of the boundary layer was set equal to $6.7\,\mathrm{m\,s^{-1}}$. We have assumed that the velocity profile has a logarithmic form (Eq. 1) and we have computed the values of roughness height $z_0$, friction velocity $u_*$ and displacement height $d$ from the measured mean velocity profiles. Raupach et al. (2006) review the different methods that can be used to estimate $u_*$; we have estimated it from the relationship $u_* = \sqrt{\overline{u'w'}}$ by averaging the $\overline{u'w'}$ data in the lower part of the flow field, where the Reynolds stresses vary only slightly with respect to their average value. The two other parameters, $z_0$ and $d$, are then estimated through the best fit of the mean velocity profile with a logarithmic law, assuming the computed value of $u_*$. The estimates of incertitude for $d$ and $z_0$ were obtained from stochastic simulations of the data, using the known incertitudes for $U$, $u_*$ and $z$.

The results (mean vales and r.m.s. for each parameter) in Table 1 show that, as the aspect ratio $(H/W)$ decreases, the roughness length tends to increase, but this is most marked when the flow regime changes from skimming flow to wake-interference flow. Adding small-scale roughness elements increases the roughness length, but their influence diminishes as the aspect ratio decreases. The most plausible physical explanation for this is that when the obstacles are relatively close together ($H/W$ large — skimming flow) the flow in the boundary layer is unable to penetrate to the bottom of the cavity, so the effect on the boundary-layer profiles is independent of cavity depth. In the wake-interference regime the roughness length is entirely determined by the large-scale obstacles, and the small roughness does not change it; the flow dynamics in the lower part of the boundary layer are then dominated by larger scale structures (of the order of the obstacle height, $H$) that engulf and dissipate the smaller scale structures generated by the smaller roughness elements.

### 3.2 Wall Similarity in the Outer and Inertial Regions

A further analysis of the results was concerned with their consistency with the assumption of *wall similarity*; the turbulent motion above a rough wall depends only on $u_*$ (the friction velocity) $\delta$ (the boundary-layer thickness) and $z$ (the distance from the wall) provided that the Reynolds number is sufficiently large. If this assumption is valid then the vertical profiles of all the flow variables should collapse onto a single curve in the outer region of the flow if the velocities are scaled on $u_*$ and the vertical distances are scaled on $\delta$. This means that the normalized profiles of all moments of the velocity can be expressed as invariant functions of

**Table 1** Estimation of $u_*$, $z_0$ and $d$ by a best fit of the mean velocity profiles

| Configuration | $(H/W)$ | $z_0$ (mm) | $u_*$ (m s$^{-1}$) | $d$ (mm) |
|---|---|---|---|---|
| 1a | (1) | $0.31 \pm 0.06$ | $0.33 \pm 0.01$ | 57±2 |
| 2a | (2) | $0.13 \pm 0.06$ | $0.30 \pm 0.01$ | 59±2 |
| 3a | (1/2) | $1.70 \pm 0.60$ | $0.41 \pm 0.04$ | 52±2 |
| 1b | (1) | $0.59 \pm 0.12$ | $0.36 \pm 0.01$ | 61±1 |
| 2b | (2) | $0.350 \pm 0.03$ | $0.34 \pm 0.01$ | 61±1 |
| 3b | (1/2) | $1.70 \pm 0.60$ | $0.41 \pm 0.04$ | 52±2 |
| 0b | ($\infty$) | $0.35 \pm 0.03$ | $0.34 \pm 0.01$ | 61±1 |

the normalized vertical coordinate $\eta = (z - d)/(\delta - d)$. Figure 3 shows the data plotted in normalized form.

For the mean flow, this invariant function is usually referred to as the mean defect law, defined as $(U_\infty - U)/u_* = G(\eta)$. As can be seen in Fig. 3a, the data agree well with this relation; the mean velocity profiles demonstrate similar dependence on $\eta$ and they are independent of the obstacle configuration and of the measurement location (type A and type B profiles).

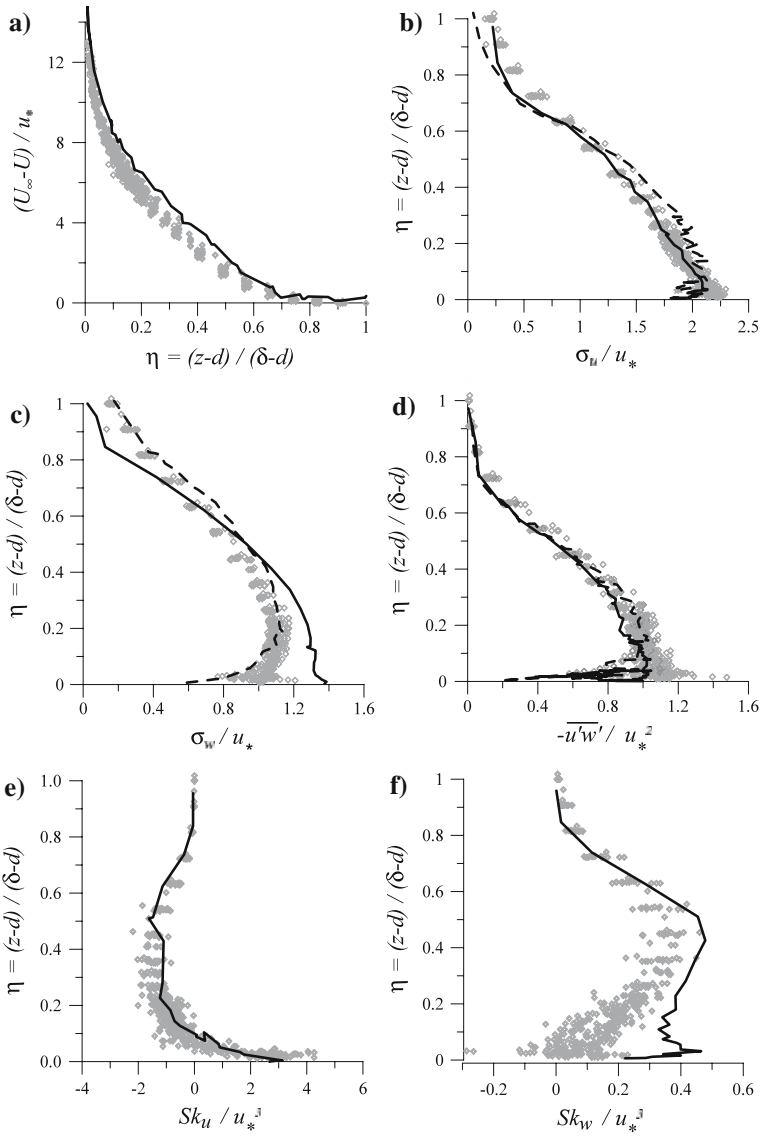


**Fig. 3** Normalized velocity profiles. (**a**) Mean velocity defect law, (**b**) $\sigma_u$ (**c**), $\sigma_w$ (**d**), $\overline{u'w'}$ (**e**), $Sk_u$ (**f**), $Sk_w$. Diamonds: data from this study; solid line: Krogstad and Antonia (1999); dashed line: Raupach et al. (1991)

The profiles for the turbulent quantities $\sigma_u$, $\sigma_w$, and $\overline{u'w'}$, as well as $Sk_u$ and $Sk_w$ (the skewness of the horizontal and of the vertical velocity respectively) show more scatter, particularly close to the ground (Fig. 3b–d), but overall the behaviour is similar in both the outer region and the inertial region $0.1 < \eta < 0.2$. The scatter close to the ground is partly due to the streamwise variation in wall roughness. In particular, the scatter in the values of $\sigma_w$, $\sqrt{\overline{u'w'}}$ and $Sk_w$ data for low values of $\eta$ is due mainly to streamwise variations in the flow, in the wake-interference flow regime; this feature is discussed Sect.3.4.

In Fig. 3 we have also plotted data obtained by Raupach et al. (1991) for flows over different kinds of wall roughness and by Krogstad and Antonia (1999) for rod-mesh roughness. Our measured profiles of $\sigma_u$, $\sigma_w$ and $\overline{u'w'}$ agree well with those presented by Raupach et al. (1991), over the whole depth of the boundary layer. The measured profiles also agree well with the data of Krogstad and Antonia (1999) for the mean velocity defect law (Fig. 3a), the second- and third-order moments of the horizontal fluctuating velocity (Fig. 3b, e) and for the Reynolds stress (Fig. 3d). However there are significant differences between the measured profiles of the vertical fluctuating velocities and those reported by Krogstad and Antonia (1999) for both the second- and third-order moments (Fig. 3-c, f). The differences in the profiles of $\sigma_w$ are probably related to the differences that are also evident in the profiles of the skewness of the vertical velocity (Fig. 3f). Krogstad and Antonia (1999) suggested that the skewness of the vertical velocity represented the dominant diffusion term for the fluctuating vertical velocities $\sigma_w$, and the values of $Sk_w$ measured by them in the region close to the wall do indeed correspond to a flatter profile of $\sigma_w$, indicating a more rapid diffusion of $\sigma_w$. This result illustrates that the second and the third moments of the vertical velocity are very sensitive to the geometry of the wall. They also show that flows with different wall roughness can have the same Reynolds stress and mean velocity profiles, but different r.m.s. velocity fluctuations. As pointed out by Antonia and Krogstad (2001), this provides experimental evidence of the limits of the similarity theory.

## 3.3 Skimming Flow Regime

### *3.3.1 The influence of small-scale roughness*

The measurements of roughness length as a function of the aspect ratio (Table 1) show that the small-scale roughness has the greatest influence in the skimming flow regime. To investigate this in more detail, we have compared the velocity profiles for the flow regime $without$ small-scale roughness (Configurations 1a and 2a) with the corresponding velocity profiles for the case $with$ small-scale roughness (Configurations 1b and 2b). We also compare the profiles measured above the obstacles (Type A) with those measured above the cavity (Type B). The mean velocity profiles for the two configurations are plotted in Figs. 4a, 5a. The first important conclusion from these profiles is that the mean velocity profile varies very little between the two positions, and the addition of small-scale roughness to the obstacle surfaces has a much greater effect. In fact this feature indicates slight interaction between the cavity and the overlying boundary-layer flow, and this is also evident in the profiles of fluctuating velocities; this is discussed further at the end of this section. However, the streamwise variability is not evident in the higher moments of the streamwise velocity as can be seen in the profiles of the two horizontal velocity (Figs. 4b, 5b) and in the skewness, although these profiles are not shown here.

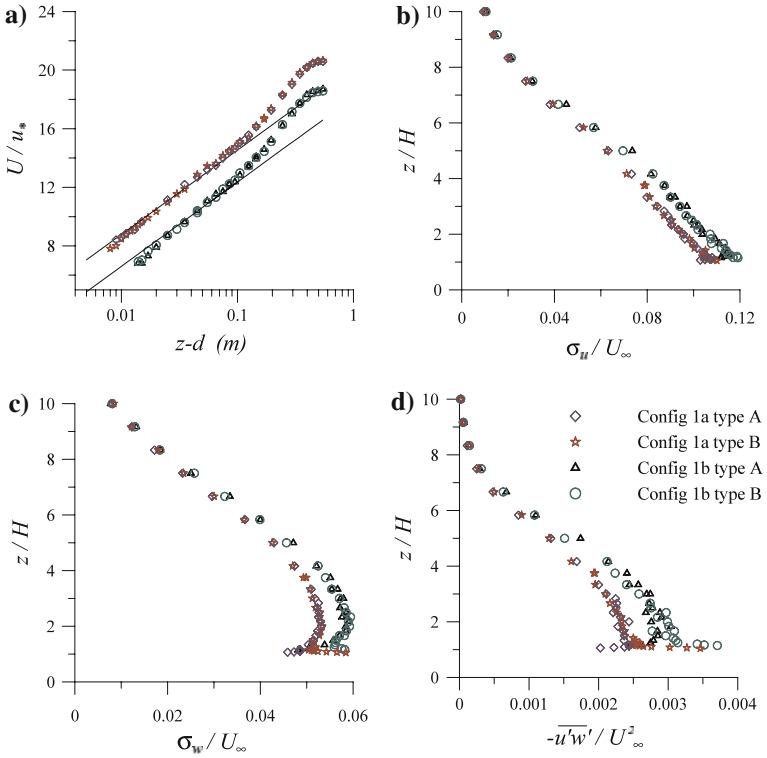


**Fig. 4** Configuration 1; dimensionless vertical profiles of (**a**) horizontal mean velocity (**b**) r.m.s. horizontal velocity (**c**) r.m.s. vertical velocity (**d**) Reynolds stress

For skimming flow, some of the profiles for Configuration 1 (r.m.s. vertical velocity, Reynolds stress—see Fig. 4) show some streamwise variability whereas none of the profiles of Configuration 2 (Fig. 5) shows any evidence of streamwise variability.[1]

Other differences between the two configurations are evident when the profiles of turbulent quantities are compared—in Configuration 1a the two profiles are noticeably different up to a height of $z/H \approx 8$, whereas in Configuration 2a the differences disappear at $z/H \approx 5$. These differences are not entirely compatible with the notion of wall similarity; in both Configurations 1 and 2 the effect of the small-scale roughness is to increase the values of the fluctuating velocities in the lower part of the flow field by about 20%. Now from similarity theory we would expect that, if there is no variation in boundary-layer depth and blending height between Configuration 1 and Configuration 2, then the increase in the turbulence levels caused by the small-scale roughness should be the same for both configurations. However this is not the case, and we have to conclude that the small-scale roughness also affects the rate at which surface-generated turbulence is transported away from the surface. This

[1] It should be noted that, in Configuration 2, the absence of streamwise variations is evidence of an anomaly in the Reynolds stress profiles close to the surface, where the Reynolds stress appears to decrease. This is certainly unphysical; the high shear in this region should lead to an increase in Reynolds stress, and this has indeed been observed in many experimental studies (Mulhearn and Finnigan 1978; Mulhearn 1978; Raupach et al. 1980). The most likely explanation for this is a measurement error due to the probe velocity acceptance angle (±45°), as documented by Perry et al. (1986).

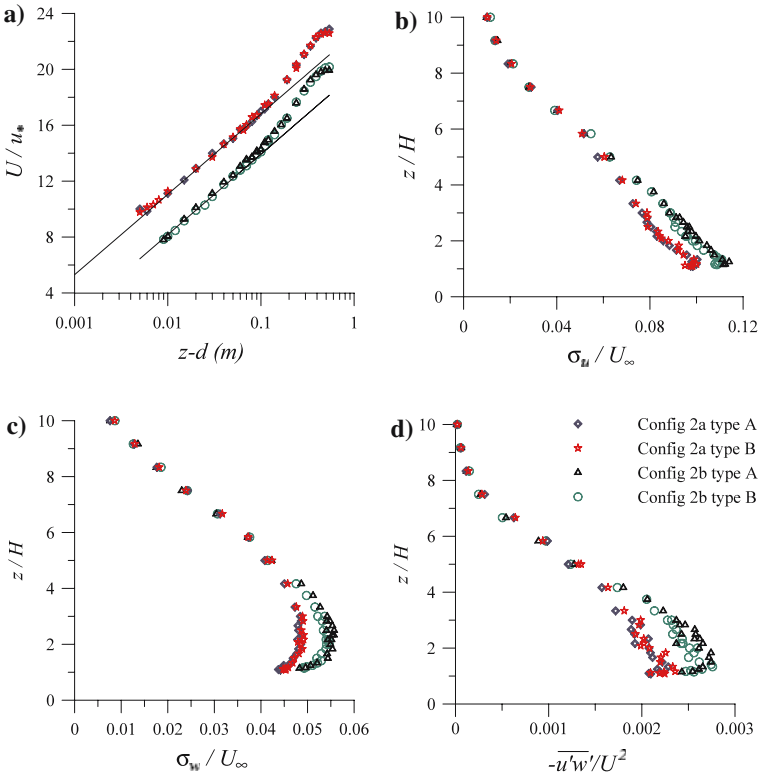


**Fig. 5** Configuration 2; dimensionless vertical profiles of (**a**) horizontal mean velocity (**b**) r.m.s. horizontal velocity (**c**) r.m.s. vertical velocity (**d**) Reynolds stress

should be visible in differences in the spectral representation of the turbulence for the two configurations. This diffusion of turbulence will depend principally on the large-scale eddies in the boundary-layer so it seems reasonable to conclude that these contain more energy in Configuration 1a than in Configuration 2a—this is probably part of the reason for the higher turbulence levels in Configuration 1a than Configuration 2a.

The general behaviour of the third moments of the velocity is similar to that observed for the second moments; the profiles of the skewness of the vertical velocity $Sk_w$ (Fig. 6b) show a higher spatial variability than the profiles of the skewness of the horizontal velocity $Sk_u$ (which are not shown here). The addition of small-scale roughness increases the absolute values of $Sk_u$ over the whole depth of the boundary layer (Fig. 6a), even if it has very little effect in the lowest part of the flow field. The effect of the small roughness on the skewness of the vertical velocity $Sk_w$ (Fig. 6b) is much more marked; the skewness is reduced—almost to zero—over the obstacle and greatly enhanced in the outer part of the boundary layer. In this sense, lower values of $Sk_w$ in the case of Configuration 1a (compared with Configuration 1b) suggest that the small-scale turbulence generated by the small roughness partially 'shelters' the cavity from the external flow, reducing the intermittency of the momentum exchange.

Finally, it is worth noting that, in the skimming flow regime, the roughness sub-layer (the region where horizontal inhomogeneities appear) is very thin, compared with the obstacle height $H$, and the small roughness elements do not seem to thicken it significantly. A rough

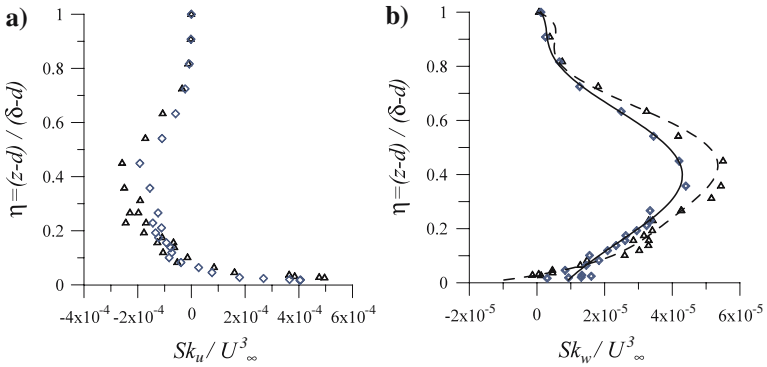


**Fig. 6** Configuration 1a (diamonds) vs Configuration 1b (triangles). (**a**) Profiles of $Sk_u$ over the obstacle (Type A) with and without small-scale roughness. (**b**) Profiles of $Sk_w$ over the obstacle (Type A) with and without small-scale roughness, the experimental curves are fitted by means of a fourth-order polynomial—solid line for Configuration 1, dashed line for Configuration 1b

estimation of the blending height can be obtained by analyzing the profiles of the turbulent quantities; we can consider that $z_* \sim (7/6)H$ in Configuration 1a and $z_* \sim H$ for Configuration 2a (non streamwise variations could be detected). In fact, the depth of the roughness sub-layer is of the order of $(H - d)$, which can be assumed to provide a rough estimate of the length scale of typical vortical structures shed by the shear layer at the top of the cavity. This feature suggests weak interaction between the cavity flow and the external boundary-layer flow, implying that the characteristic time scale ($T_t$) for boundary-layer flow close to the surface ($z = H$) is much longer than the time scale for the transit across the cavity ($\sim W/U_{loc}$).

### *3.3.2 Configuration 0b*

As the spacing between the obstacles decreases ($W \to 0$), the ratio $H/W \to \infty$, and the flow becomes identical to that over a continuous flat plate, with a displacement height $d$ equal to the obstacle height (the origin of the velocity profile is taken at the base of the obstacles). For the case of small roughness elements on large obstacles the limiting case for $H/W \to \infty$ is therefore small roughness elements on a flat plate, located at a height $H$ above the base of the obstacles. This corresponds to Configuration 0b, which is therefore the limiting case ($H/W \to \infty$) for the skimming flow regime. It is instructive to compare the profiles for Configuration 0b with those for Configuration 2b, to isolate the influence of the small-scale roughness.

Firstly, the mean velocity profiles for the two configurations are almost identical (Fig. 7a, b) showing that for skimming flow with $H/W = 2$ the displacement height has become equal to the obstacle height (Rafailidis 1997). The profiles of horizontal fluctuating velocities $\sigma_u/U_\infty$ and $\sigma_w/U_\infty$ are very similar (Fig. 7d, e)—there is very little difference between the profiles over the cavity and the obstacle (2b type A and 2b type B) and the profile for the small-scale roughness (0b). Even the Reynolds stress profiles for Configuration 2b (Types A and B) and Configuration 0b do not seem to differ significantly from each other (Fig. 7c). In fact, if we accept that the average Reynolds stress in this lower part of the boundary layer does not differ much between the three profiles, then it follows that the drag exerted by the boundary on the flow does not vary much either, and therefore that the cavity does not have

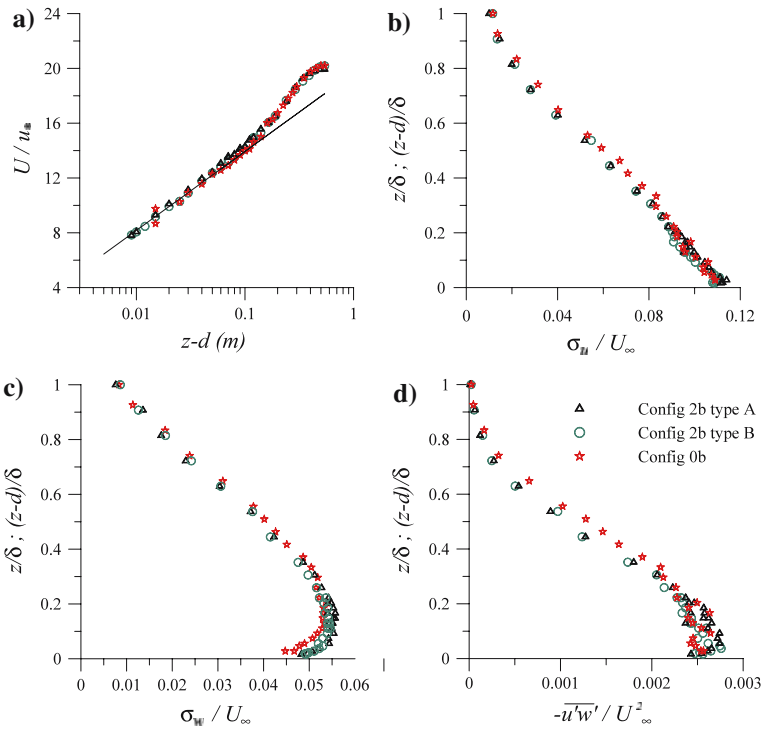


**Fig. 7** Configuration 0b and Configuration 2b; (**a**) mean horizontal velocity; (**b**) r.m.s. horizontal velocity; (**c**) r.m.s. vertical velocity (**d**) Reynolds stress

any influence on the drag. This agrees with the idea proposed by Perry (1968) that in the skimming flow regime all flow variables (blending height, effective roughness length, friction velocity, etc) should be independent of the ratio $H/\delta$.

### 3.4 Wake-interference Flow

The velocity profiles for the wide cavity (Configuration 3a, $H/W = 1/2$) are very different from those for the narrower cavities (Configurations 1a and 2a, with $H/W = 1$ and $H/W = 2$ respectively) and this is indicative of a major change in the flow regime (Fig. 8).

The small-scale roughness appears to have hardly any influence on the characteristic velocity profiles; only the profile of average horizontal velocity shows any discernible and consistent difference (Fig. 8a). The additional small-scale roughness reduces the vertical gradient of the horizontal velocity in a region very close to the wall, compared with the standard logarithmic profile, and the depth of this region is of the same order as the height of the roughness element ($h$). This may be due to an enhanced diffusion of momentum, confined to a very thin layer immediately above the obstacles. This is the only discernible effect of the small-scale roughness; all the other profiles (Reynolds stress, $\sigma_u$, $\sigma_w$—Fig. 8 b, d) seem to be insensitive to the presence of small-scale roughness. It is possible that instabilities generated within the shear layer at the interface between the cavity and the external flow have sufficient space to evolve and grow to envelope and dissipate the smaller scale structures that are generated by the small roughness elements. In this case the boundary layer is dominated by

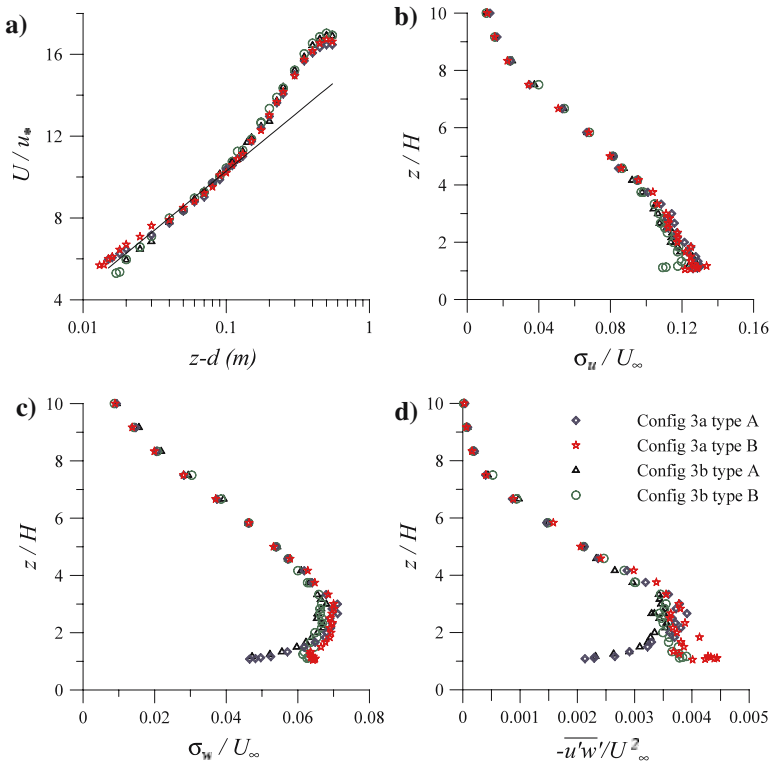


**Fig. 8** Configuration 3; dimensionless vertical profiles of (**a**) horizontal mean velocity (**b**) r.m.s. horizontal velocity (**c**) r.m.s. vertical velocity (**d**) Reynolds stress

the dynamics of the larger eddies, with typical length scales which are large in comparison with the small roughness dimension.

The profiles of Reynolds stress (Fig. 8d) and r.m.s. of vertical velocity (Fig. 8c) show significant streamwise variations, but no such variation can be detected in the profiles of horizontal mean velocity (Fig. 8a).

## 4 Conclusions

Wind-tunnel experiments have been performed to investigate the influence of small-scale roughness elements on the flow above a series of street canyons for a range of canyon aspect ratios.

The velocity measurements were analyzed in order to define the validity and limitations of the similarity theory. In general, the scaling of the velocity profiles agrees well with that stated by the theory. However, as already observed by previous researchers (Antonia and Krogstad 2001), the different turbulent quantities behave differently for different wall geometries: this is the case for the second- and third-order moments of the vertical velocity, which show more scatter than the corresponding moments of the longitudinal velocity.

The extent of the RSL varies significantly from one regime to the other. In the case of wake-interference flow (k-type roughness) the extent of the RSL is much larger and appears

to be proportional to the obstacle height, i.e. $z_* \sim 2H$. On the other hand, in the case of skimming flow (d-type roughness), the vertical extension of the RSL is much smaller than $H$ and could be considered almost negligible when compared with the boundary-layer height. The experiments confirm the observation of Perry et al. (1968), that, for $H/W > 1$, the roughness element height $H$ is not a relevant length in determining the characteristic roughness length $z_0$ of the wall.

As a general conclusion, the dynamics of a turbulent boundary layer over a surface with two roughness scales are mainly related to only one roughness length. In the case of high aspect ratio cavities ($H/W > 1$), the small-scale roughness increases the turbulence intensity and the turbulent momentum transfer. In these conditions, the smaller scale structures produced by the small-scale roughness influence the flow dynamics as long as their size is of the same order as that of the eddies shed by the shear layer developing at the canopy top. The extent of the region influenced by the small-scale roughness depends on the cavity aspect ratio $H/W$, and this variability demonstrates the limitations of the similarity theory. In the case of wider cavities (for $H/W < 1$), the effect of the smaller scale roughness is no longer evident and the flow is presumably dominated by the larger scale shear-induced eddies (with linear dimension $\sim H$), which are generated at the top of the cavities. We could expect these conclusions to be valid also in the case of three-dimensional geometries and of less regular obstacle arrays. As a general criterion we suggest that the small-scale roughness has an influence on the flow dynamics only in the skimming flow regime. Even in that case however, we expect that the small roughness will have an influence only if its size exceeds the quantity $H - d$, which can be considered as a rough estimate of the eddies size in the lowest part of the boundary layer.

## References


Antonia RA, Krogstad PA (2001) Turbulence structure in boundary layers over different types of surface roughness. Fluid Dyn Res 28:139–157

Athanassiadou M, Castro IP (2001) Neutral flow over a series of rough hills: a laboratory experiment. Boundary-Layer Meteorol 101:1–30

Counihan J (1969) An improved method of simulating an atmospheric boundary layer in a wind tunnel. Atmos Env 3:197–214

Gong W, Taylor PA, Dörnbrack A (1996) Turbulent boundary-layer flow over fixed aerodynamically rough two-dimensional sinusoidal waves. J Fluid Mech 312:1–37

Irwin HPAH (1981) The design of spires for wind simulation. J Wind Eng and Indust Aerod 7:361–366

Krogstad PA, Antonia RA (1999) Surface roughness effects in turbulent boundary layers. Expts Fluids 27:450–460

Mulhearn PJ (1978) Turbulent flow over a periodic rough surface. Phys Fluids 21(7):1113–1115

Mulhearn PJ, Finnigan JJ (1978) Turbulent flow over a very rough random surface. Boundary-Layer Meteorol 15:109–132

Nikuradse J (1933) Strömungsgesetze in rauhen Rohren. Forschg Arb Ing-Wes 361:1–22

Oke TR (1987) Boundary layer climates. 2nd edn. Methuen, London 435 pp

Perry A, Lim K, Henbest S (1986) An experimental study of the turbulence structure in smooth- and rough-wall boundary layers. Fluid Mech 177:437–466

Perry A, Shofield WH, Joubert PN (1968) Rough wall turbulent boundary layers. J Fluid Mech 37:383–413

Rafailidis S (1997) Influence of building areal density and roof shape on the wind characteristics above a town. Boundary-Layer Meteorol 85:255–271

Raupach MR (1992) Drag and drag partition on rough surfaces. Boundary-Layer Meteorol 60:375–395

Raupach MR, Antonia R, Rajoplan S (1991) Rough-wall turbulent boundary layers. Appl Mech Rev 44(1): 1–25

Raupach MR, Hughes HA, Cleugh DE (2006) Momentum absorption in rough-wall boundary layers with sparse roughness elements in a random and clustered distributions. Boundary-Layer Meteorol 120: 201–218

Raupach MR, Thom AS, Edwards I (1980) A wind-tunnel study of turbulent flow close to regularly arrayed rough surfaces. Boundary-Layer Meteorol 18:373–397

Soulhac L (2000) Modélisation de la dispersion atmosphérique à l'intérieur de la canopée urbaine. Ph.D. thesis, Ecole Centrale de Lyon

Tennekes H, Lumley JL (1972) A first course in turbulence. The MIT Press, 300 pp